J. metamorphic Geol., 2002, **20,** 481–492

Silica precipitates in omphacite from eclogite at Alpe Arami, Switzerland: evidence of deep subduction

L. F. DOBRZHINETSKAYA,[1] R. SCHWEINEHAGE,[2] H.-J. MASSONNE,[2] AND H. W. GREEN[1]
[1]*Earth Sciences Department and Institute of Geophysics and Planetary Physics, University of California, Riverside, CA, 92521, USA (larissa@ucrac1.ucr.edu)*
[2]*Institut für Mineralogie und Kristallchemie, Universität Stuttgart, Azenbergstrasse 18, D-70174 Stuttgart, F.R. Germany*

ABSTRACT Observations of oriented SiO_2 precipitates in omphacite from eclogite with tholeiitic basalt protolith bordering the Alpe Arami garnet peridotite massif, Ticino, Switzerland, and petrological studies of the eclogitic mineral assemblages, suggest that this rock was subjected to higher-pressure metamorphism than previously realized. We employed various calibrations of the $Fe^{2+}-Mg$ exchange thermometer and calculations of equilibria with thermodynamic data, considering the calcium–Tschermak's component ($CaAl_2SiO_6$), of garnet-pyroxene pairs. From these calculations, it is concluded that the eclogitic lenses have recorded at least four stages of mineral growth corresponding to the following: Stage I (prograde) *c.* 2.4 GPa; 700 °C; Stage IIa (maximum recorded grade) *c.* 7.0 GPa; 1100 °C; Stage IIb (retrograde) *c.* 3.7 GPa; 900 °C; Stage III (retrograde) *c.* 2.1 GPa; 750 °C. Because of the preservation of Stage I, a relatively rapid subduction and exhumation of Alpe Arami eclogite is suggested. The exhumation path of the eclogitic rock is in good agreement with most exhumation paths inferred for the Alpe Arami garnet lherzolite proposed previously by several authors based upon a variety of different observations, although the eclogite and peridotite exhumation paths may diverge at depths greater than 120 km.

Key words: Alpe Arami, eclogite, omphacite, ultra-high pressure.

INTRODUCTION

We have recently discovered oriented SiO_2 precipitates in omphacite from eclogite bordering the Alpe Arami (AA) peridotite massif in Ticino, Switzerland (Green *et al.*, 2000; Dobrzhinetskaya *et al.*, 2000b). To our knowledge, such evidence for Si-rich clinopyroxene has not been described previously from the AA, nor from elsewhere in the Alps. However, omphacite with precipitates of SiO_2 is well-known from eclogite xenoliths in kimberlite pipes (e.g. Smyth, 1980) and from many eclogites of other continent-continent collisional metamorphic belts, e.g. the Western Gneiss Region, Norway (Smith & Cheeney, 1980, 1988), the Bohemian Massif, (e.g. in the Sudetes, Poland; Bakun-Chubarow 1992) and the Münchberg Massif, Germany (Gayk *et al.*, 1995), the Sulu region, China (Zhang *et al.*, 1995), and the Kokchetav Massif, Kazakhstan (Katayama *et al.*, 2000). Tsai (1998) has also reported abundant SiO_2 rods in sodic augite/Na-bearing diopside ($Fe:Mg:Ca = 14.2/39.3/46.5$, $Na_2O = 1.55$ wt%) from eclogite of the Dabie Mountains, China. In all cases, SiO_2 needles and rods in omphacite have been interpreted as exsolution products from a Si-rich clinopyroxene. Smyth (1980) suggested that deviations from stoichiometry are reconciled by allowing up to 9% vacancy in the M2 site, and that the vacancies are stabilized by pressure in excess of 3 GPa but are highly unstable at lower pressure. Later, Smith, 1988 suggested that crystallization of such clinopyroxene requires both high pressure and high temperature.

Most, if not all, eclogites containing omphacite with SiO_2 precipitates occur in association with garnet peridotites and other rocks showing evidence of very high pressure, recorded, for instance, by the presence of metamorphic diamonds (Kokchetav massif of Kazakhstan, Sobolev & Shatsky, 1990; Dabie Mountains of China, Xu *et al.*, 1992; Western Gneiss Region of Norway, Dobrzhinetskaya *et al.*, 1995; NW Bohemian Massif, Germany, Massonne, 1999), thermobarometric evidence of pressures as high as 6 GPa (China, Yang *et al.*, 1993), and pyroxene exsolution from garnet (Western Gneiss Region, Van Roermund & Drury, 1999; China, Ye *et al.*, 2000). Our previous work on the AA garnet lherzolite is consistent with pressures as high as 8 to 10 GPa (Bozhilov *et al.*, 1999; Dobrzhinetskaya *et al.*, 1996, 2000a). These observations on natural rocks suggest that the pressure at which SiO_2-rich clinopyroxene is stabilized is probably not less than 4 GPa.

Available experimental studies show that the presence of topotaxially related SiO_2 rods in omphacite

can be explained by exsolution from nonstoichiometric SiO_2-rich precursors stabilized at very high pressure conditions. The earliest experiments (Mao, 1971) showed that jadeite–calcium-Tschermak's clinopyroxene may dissolve up to 7.5% excess SiO_2 at 4 GPa, and 1100–1700 °C and that the solubility of SiO_2 in such clinopyroxene increases with pressure. Similar experimental observations were also obtained from diopside–calcium-Tschermak's clinopyroxene at 2.5–3.2 GPa, 1400–1500 °C (Wood & Henderson, 1978), and from diopside–calcium-Eskola ($Ca_{0.5}AlSi_2O_6$) clinopyroxene at 3.5–7 GPa, 1200 °C (Zharikov *et al.*, 1984). More recently, Angel *et al.* (1988) showed that a nonstoichiometric silica-rich Na-Mg pyroxene with six-co-ordinated silicon is stable at 10–15 GPa, 1600 °C.

Described here are the results of our petrological analysis of the eclogite mineral assemblages associated with omphacite containing abundant SiO_2 precipitates collected from the eclogite body at Alpe Arami. The thermobarometric results record a tight burial/exhumation loop that extends to 7 GPa (*c.* 220 km depth in Earth) when the SiO_2 rods are calculated as part of the pyroxene chemistry. The *P–T* path is in good agreement with *P/T* points (Ernst, 1981; Medaris & Carswell, 1990) and exhumation curves (Brenker & Brey, 1997; Dobrzhinetskaya *et al.*, 1996; Bozhilov *et al.*, 1999; Green *et al.*, 2000) previously reported for the associated AA peridotite.

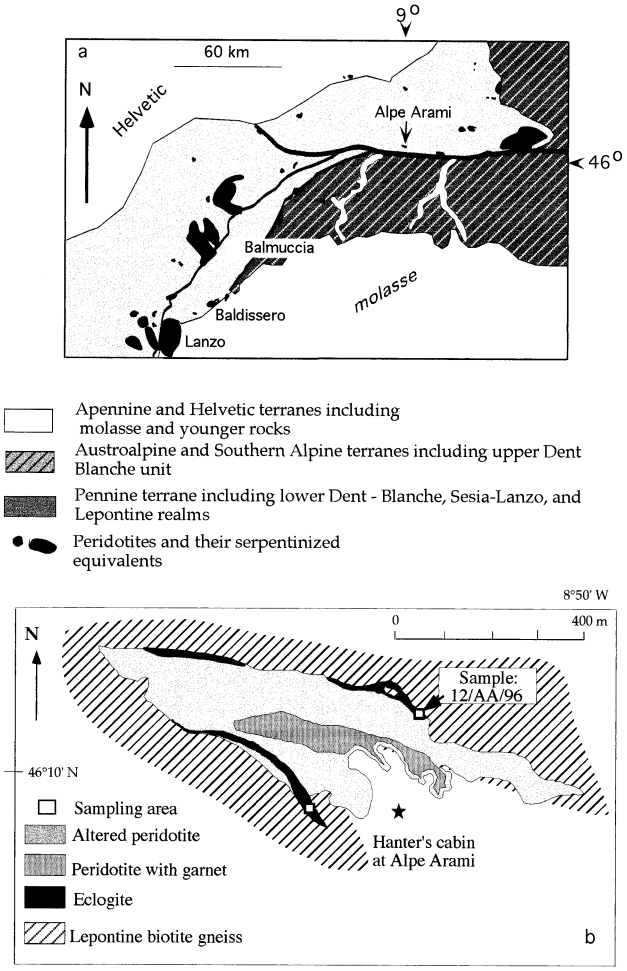

Fig. 1. Geological schemes: (a) Regional geological scheme of the western Alps, simplified from the 1 : 500 000 scale map sheet 1 of the Structural Model of Italy (G. Bigi, D. Cosentino, M. Parotto, R. Saratori & P. Scandone, scientific co-ordinators and editors, Italy, 1990); (b) Geological scheme of the Alpe Arami peridotite massif and associated eclogite, modified after Möckel (1969).

GEOLOGICAL BACKGROUND

At Alpe Arami in the western Alps, eclogites occur as thin, partly discontinuous, lenses surrounding a garnet-lherzolite body (see Fig. 1a,b). This eclogitic layer tends to separate the AA garnet peridotite massif from the surrounding strongly migmatized quartzo-feldspathic Lepontine gneisses (Möckel, 1969; Ernst, 1977). There is a discordance in schistosity between eclogite and Lepontine gneisses (Möckel, 1969) as well as evidence of mylonitization (Buiskool Toxopeus, 1977). Although the contact between eclogite and garnet-peridotite looks to be concordant according to the interpretation of the geological map (Möckel, 1969), there is no direct evidence demonstrating that these two units were in close association before their mutual deformation and recrystallization during the Alpine orogeny. Most observations indicate that AA garnet-peridotite was tectonically emplaced from the upper mantle with its garnet-bearing assemblage intact. We show below that comparison of the eclogite and peridotite *P/T* trajectories suggests that they came into contact before or during Alpine time, perhaps during Alpine exhumation. The rocks were subsequently modified by Alpine metamorphism and deformation (Möckel, 1969; Ernst, 1978, 1981; Medaris & Carswell, 1990; Dobrzhinetskaya *et al.*, 1996, 2000a; Brenker & Brey, 1997; Bozhilov *et al.*, 1999). These publications are generally in agreement with respect to the exhumation history of the peridotite, except for the proposed depth from which exhumation began: 100–120 km (Ernst, 1978, 1981), 150 km (Medaris & Carswell, 1990), >160 km (Brenker & Brey, 1997), >300 km (Dobrzhinetskaya *et al.*, 1996, 2000a), >250 km (Bozhilov *et al.*, 1999). A few recent publications dismiss the varied lines of evidence that suggest very great depths and propose maximum pressures <4 GPa (Arlt *et al.*, 2000; Risold *et al.*, 2001; Nimis & Trommsdorff, 2001a). The two most recent contributions to this discussion (Nimis & Trommsdorff, 2001a; Paquin & Altherr, 2001a) both make extensive use of thermobarometry of the AA peridotite. Unfortunately, these two papers do not resolve the controversy that surrounds this body because the former calculates a maximum pressure and temperature lower than all previous workers (3.2 GPa; 850 °C) whereas the latter calculates *P–T* higher than all previous users of this method (5.9 GPa; 1200 °C). Many of the fundamental discrepancies between the results of Nimis & Trommsdorff (2001a) and Paquin & Altherr (2001a) are addressed in their recent discussion and reply (Nimis & Trommsdorff, 2001b; Paquin & Altherr, 2001b) and need not be discussed further here. Clearly, additional information should be useful in addressing this important subject.

The AA eclogites are characterized by roughly basaltic bulk chemistry (Grubenmann, 1908; O'Hara & Mercy, 1963). Their REE patterns indicate a tholeiitic magma protolith (Ernst, 1981). Eclogitic mineral assemblages are represented by garnet + omphacite + rutile + kyanite, which are partly replaced by amphibolite facies mineral associations (pargasitic amphibole, clinozoisite, intermediate plagioclase) and other low *P–T* retrograde minerals such as chlorite,

actinolite, biotite and varying amounts of quartz (Möckel, 1969; Ernst, 1977, 1981). Employing various geothermometers and geobarometers, Ernst (1981) computed that eclogites from AA were crystallized at 900 °C and 4 GPa. Ernst (1977) also indicated (p. 394) that: 'Clearly these eclogitic rocks seem to have been generated at much more profound depth than those from nearby Cima di Gagnone (Evans & Trommsdorff, 1975; Trommsdorff *et al.*, 1975)'.

MATERIALS AND METHODS

Samples and preparation

Eclogite samples were collected at AA from both the northern and southern margins of the garnet-lherzolite (see Fig. 1b). They are medium-grained, pinkish-greenish, massive or foliated rocks composed predominantly of pale red garnet and pale green pyroxene with minor kyanite. Alteration products are represented by finer-grained amphibolite-greenschist facies mineral assemblages. Polished thin sections of 40 μm thickness were prepared for investigation by optical and scanning electron microscopy (SEM) and electron microprobe (EMP). Omphacite with SiO_2 precipitates was discovered in several thin sections from both northern and southern eclogite layers. Sample 12/AA/96, collected near the northern contact with the garnet-peridotite along the path which runs to the NNE from the AA hunter's cabin (see Fig. 1b), was chosen for detailed analytical study.

Analytical techniques

Chemical compositions of minerals were determined with the four wavelength dispersive spectrometers of a CAMECA SX50 electron microprobe. Nearly 100 spot analyses were performed using an acceleration voltage of 15 kV and a beam current of 30 nA. Counting times were 20 s per element for the peak and 10 s each for the background. For Ti and Cr, the peak counting times were extended to 100 s and for Mn 60 s. Standards were topaz for F, jadeite for Na, synthetic pyrope for Mg, Al and Si, a K, Ca, Mg, Al-bearing silicate glass for K, a glass of theoretical andradite composition for Ca and Fe, synthetic TiO_2 for Ti, synthetic Cr_2O_3 for Cr, synthetic spessartine for Mn, synthetic ZnO for Zn and a glass of the bulk composition $BaSiO_3$ for Ba (Lα line, Kα lines for all other elements). The PAP matrix correction provided by CAMECA was applied. The subsequent calculation of structural formulae for the different minerals is explained in the corresponding tables. The calculation of molar fractions for clinopyroxene and garnet is in accordance with Massonne (1992) because their thermodynamic data and solid solution models of clinopyroxene and garnet were used for the estimation of *P–T* conditions.

In addition to single-spot (5 μm diameter) analyses, we performed a series of spot analyses along profiles through the omphacite and garnet grains. In regions containing precipitates, some omphacite analyses were performed with an electron beam of 30 μm diameter in order to obtain a bulk composition of omphacite existing prior to precipitation. Numerous semiquantitative EDS analyses were also undertaken. Element distribution maps for Mg, Fe and Ca in the minerals were produced simultaneously through stepwise scanning with the electron beam over a rectangular area (Bernhardt *et al.*, 1995). In this case, a CAMEBAX was used with an acceleration voltage of 15 kV, a constant beam current close to 15 nA and a slightly defocused beam. Counting times were 1 s per step.

For microscopic studies, a Nikon polarizing optical photomicroscope equipped for both reflected and transmitted light, and a Philips XL30 FEG scanning electron microscope were used. The SEM was operated at 15 and 20 kV. The EDAX microanalytical system of this microscope consists of an energy dispersive spectrometer (EDS) equipped with Si detector with super-ultra-thin window, resolution of 137 eV MnK_α. The spectral data were acquired at 1500–2000 counts per second with dead time below 25%, beam current of about 1 nA, and effective spot size about 1.5 mm.

RESULTS

Observations with optical and scanning electron microscopes

Petrographic observations with the optical microscope indicate that eclogites have been subjected to at least two stages of recrystallization. The early stage is presented by the association of garnet and weakly oriented omphacite + rutile + kyanite with accessory amounts of ilmenite. Energy dispersive X-ray analysis coupled with SEM imaging showed that ilmenite is rich in geikelite component. The late-stage retrogressive metamorphism is clearly recognized by the presence of symplectitic intergrowths of clinopyroxene with amphibole in the presence of plagioclase of intermediate composition. Association of amphibole + clinozoisite + plagioclase with varying content of quartz, biotite and chlorite was also observed within products of retrogressive alteration.

Garnet contains abundant rounded micron-sized inclusions of rutile; minor apatite inclusions were also recognized. Many omphacite crystals associated with garnet consist of 'cloudy' internal zones surrounded by clear outer zones which are seen very well in transmitted light at low magnification in the optical microscope. We have also observed that in many cases the 'cloudy' areas are situated sporadically within omphacite. These 'cloudy' areas of omphacite observed under higher magnification consist of rods, needles and plates of a clear, transparent phase of low refractive index (Fig. 2a). In almost all cases, the rods/needles are elongated parallel to the [010] direction of the host omphacite (Fig. 2b). Detailed observations with secondary electrons in the SEM indicate that the rods are typically 0.1–2 μm diameter and about 3–20 μm long (Fig. 2c); platy crystals are 0.1–1 μm thickness, with width about 1 μm and length about 2 μm (Fig. 2d). Numerous EDS spectra obtained for rods, needles and plates confirm that they are essentially pure SiO_2.

Electron microprobe analysis

Garnet

Garnet grains in the sample 12/AA/96 are approximately 1 mm in diameter. Their compositions were investigated by spot analyses, radial profiles, and element distribution maps. The garnet composition (see Table 1) is that of an ordinary medium-temperature eclogite with almandine component dominating (*c.* 40 mol%), pyrope and grossular *c.* 30 mol% each, and spessartine *c.* 1 mol%. According to the calculation procedure for the structural formulae of garnet (see Table 1), the andradite component could be as high as 3 mol%. Titanium contents can reach 0.02 Ti per double formula unit whereas chromium is almost negligible in all studied samples and other element concentrations were below detection limits.

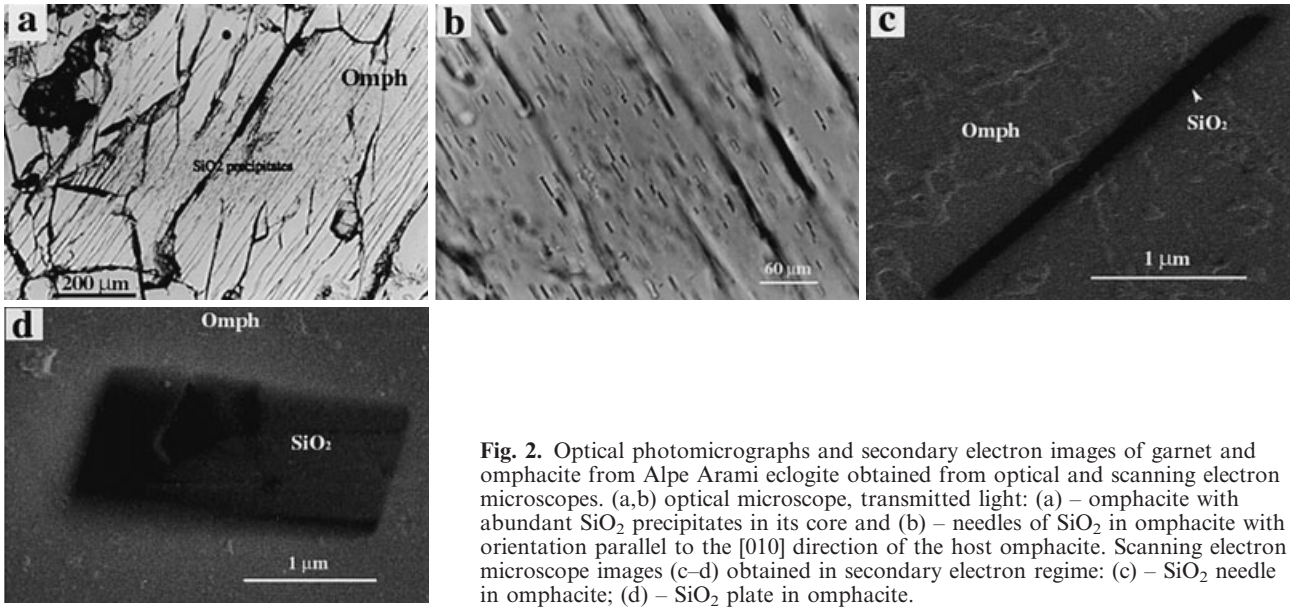

Fig. 2. Optical photomicrographs and secondary electron images of garnet and omphacite from Alpe Arami eclogite obtained from optical and scanning electron microscopes. (a,b) optical microscope, transmitted light: (a) – omphacite with abundant SiO_2 precipitates in its core and (b) – needles of SiO_2 in omphacite with orientation parallel to the [010] direction of the host omphacite. Scanning electron microscope images (c–d) obtained in secondary electron regime: (c) – SiO_2 needle in omphacite; (d) – SiO_2 plate in omphacite.

Element distribution maps show that garnet is zoned, although not with perfect concentricity (see Fig. 3). Careful examination of many zoned grains showed that the pattern of zoning does not correlate with transgranular fractures or any other obvious structures, hence we conclude that the inner zones are older than the outer ones. Therefore, we believe that the Mg-poorest and Ca-richest garnet composition, found in the inner parts of garnet grains, is the correct representative for the earliest stage of growth; this composition has been used for Stage I of the thermobarometric calculations (see Table 1, analysis no. 16). During subsequent garnet growth, Ca decreased and Mg increased. The intermediate Ca and Mg contents of garnet (see Fig. 3c) were chosen representative of Stage II.

As discussed in more detail in the next section, the omphacite we associate with the Stage II garnet is that which contains the SiO_2 precipitates. Consideration of that pyroxene with and without recalculation of composition to account for the exsolved material causes us to identify Stages IIa (see Table 2, analysis no. 6 N) and IIb (see Table 2, analysis no. 22). There is no comparable evidence for division of garnet compositions into these two substages, but the thermobarometric calculations that follow are quite insensitive to garnet composition, hence *P–T* determinations are little effected by this uncertainty. Following Stage II, an event (dissolution?) apparently occurred that resulted in irregularly shaped grains, leaving their older 'cores' not necessarily in their geometric centres. The late, retrograde, stage of growth (Stage III) followed this event, leading to the appearance of the outermost zone that, however, did not entirely envelope the older garnet. Stage III of garnet growth (see Table 1, analysis no. 19) is characterized by slightly (but significantly) higher Fe contents compared to Stage II of garnet growth and by the lowest Ca content. The Ti contents of garnet are lowest for both Stages I (see Table 1, analysis no. 16) and III (Table 1, analysis no. 19).

Table 1. Representative analyses of garnet along a profile through one grain in the eclogite sample (12-AA-96). The data were obtained with the aid of an electron microprobe by equidistant steps through the profile. Structural formulae were calculated on the basis of 10 cations in the six- and eight-fold co-ordinated sites. Fe^{3+} results from $4-(Al+Cr)$. At the bottom are molar fractions of components used for thermodynamic calculations as explained in the text. Note that the core composition was not obtained in the centre of the grain (analyses no. 5, 9 and 13 are taken along the profile between 'core' and 'rim').

Analysis no.	1 rim	5	9	13	16 core	19 rim
Stage			II		I	III
SiO_2	38.83	39.08	39.12	39.03	39.01	39.39
TiO_2	0.04	0.14	0.17	0.10	0.05	0.05
Al_2O_3	22.24	21.90	21.82	22.18	22.16	22.79
Cr_2O_3	0.07	0.08	0.01	0.03	0.00	0.02
FeO	19.32	19.17	19.21	19.14	18.38	21.72
Fe_2O_3	0.32	0.63	0.93	0.36	0.52	0.00
MnO	0.46	0.38	0.46	0.38	0.40	0.62
MgO	8.23	8.10	7.93	8.07	7.91	8.01
CaO	10.22	10.36	10.61	10.56	11.44	8.76
sum oxides	99.72	99.84	100.25	99.85	99.87	101.36
Si	5.861	5.932	5.922	5.904	5.886	5.888
Ti	0.004	0.016	0.019	0.011	0.006	0.005
Al	3.955	3.919	3.893	3.955	3.941	4.016
Cr	0.008	0.009	0.001	0.004	0.000	0.002
Fe^{3+}	0.037	0.072	0.106	0.041	0.059	0.000
Mg	1.852	1.832	1.789	1.819	1.779	1.786
Fe^{2+}	2.438	2.434	2.432	2.421	2.320	2.716
Mn	0.059	0.049	0.058	0.049	0.051	0.079
Ca	1.652	1.685	1.720	1.712	1.850	1.403
Prp	0.309	0.305	0.298	0.303	0.297	0.299
Alm	0.406	0.406	0.405	0.404	0.387	0.454
Sps	0.010	0.008	0.010	0.008	0.009	0.013
Grs	0.275	0.281	0.287	0.285	0.308	0.234
XAl	0.989	0.980	0.973	0.989	0.985	1.000

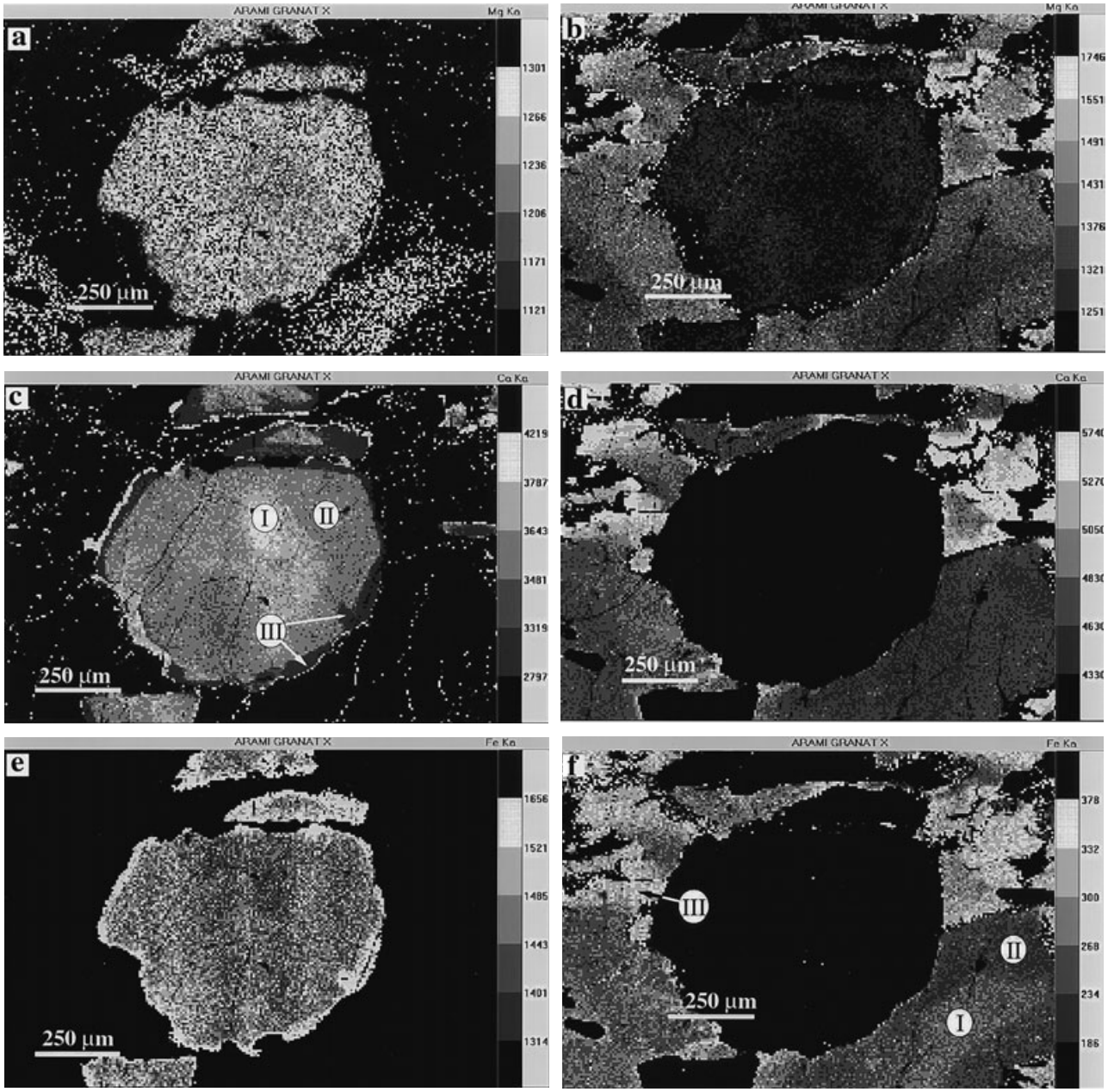

Fig. 3. Representative element distribution maps of garnet (a,c,e) as well as surrounding omphacite and its decomposition products, amphibole (b,d,f) obtained with the electron microprobe. Grey code in counts per second is at the right margin of each panel. Zones of significantly different compositions are labelled in panels (c) and (f) and correspond to metamorphic Stages I–III. Mg-Kα radiation (a & b): in garnet, the lowest concentration of Mg is located in the interior of the illustrated grain, with higher concentration in a broad outer border (a,b); in omphacite, the Mg content in the cores of grains is approximately equal to the outer border of garnet, with greater amounts in broad rims of the omphacite (shown most clearly by the grain in the lower right corner of panel b). Ca-Kα radiation (c & d): in garnet (c), Ca distribution exhibits zonal patterns closely similar to those of Mg, but with the intensities reversed (highest in the (off-centre) core, Zone I) and, in addition, it shows a well-defined but discontinuous narrow rim that exhibits lowest concentration (Zone III); concentrations in omphacite are more homogeneous in Zones I and II and show the higher amounts in the grain labelled III in panel (f); the brightest areas in (d) are secondary amphibole. Fe-Kα radiation (e & f): in garnet (e), the distribution of Fe is less clearly shown in the interior of the grain than for Mg or Ca, with the exception that the lowest (core) and highest (rim) concentrations clearly anticorrelate with the highest and lowest Ca concentrations; omphacite (f) shows highest concentration in zone III and lowest in zone II.

Omphacite

Omphacite contains, according to the calculation procedure (Table 2), somewhat more than 50 mol% of diopside + hedenbergite (hedenbergite component is minor) as well as around 45 mol% of jadeite + acmite (acmite component is minor). MnO and Cr_2O_3 contents are below 0.1 wt%. TiO_2 concentrations are around 0.2 wt%. Potassium levels are very low; other elements which are not related to the components mentioned above are below detection limits. There is a deficiency of Si referred to 2 Si per ideal clinopyroxene formula unit according to the calculated structural formulae of the studied omphacite grains. The deficiency was balanced by tetrahedrally co-ordinated Al assigned to the calcium–Tschermak's component ($CaAl_2SiO_6$).

Omphacite is only slightly variable in composition. Nevertheless, three compositional zones were detected. Zone I is related to the early growth of this mineral, and it is somewhat enriched in Fe (see Fig. 3f) and depleted in Mg.

Table 2. Representative analyses of omphacite along a profile through one grain (Fig. 4b) and of amphibole in the eclogite sample (12-AA-96). The data were obtained with the aid of an electron microprobe. Structural formulae for clinopyroxene were calculated on the basis of 4 cations and 12 valencies to obtain Fe^{3+}. For amphibole 13 cations without Ca, Na and K for the tetrahedral and octahedral sites and altogether 46 valencies were considered to calculate Fe^{3+}. The ideal value of 2.07 wt.% H_2O was taken into account to calculate the sum of oxides for amphibole. At the bottom are molar fractions of clinopyroxene components used for thermodynamic calculations as explained in the text.

Analysis no.	20 rim	22	25 core	6 N Integral analysis including Qtz rods	33 Amphibole
Stage	III	IIb	I	IIa	
SiO_2	55.13	55.04	56.04	56.58	42.99
TiO_2	0.14	0.14	0.14	0.24	0.80
Al_2O_3	11.73	11.69	11.99	11.72	14.55
Cr_2O_3	0.02	0.07	0.07	0.03	0.13
Fe_2O_3	0.38	0.00	1.55	0.00	4.10
FeO	2.85	3.16	1.76	3.08	5.95
MnO	0.06	0.04	0.01	0.03	0.07
MgO	8.55	8.31	8.63	8.41	13.89
CaO	14.26	14.29	14.06	13.75	10.53
Na_2O	6.38	6.22	6.89	6.94	4.03
K_2O	0.01	0.00	0.01	0.00	0.04
sum of oxides	99.53	99.15	101.15	100.78	99.15
Si	1.965	1.970	1.962	1.987	6.233
Al^{IV}	0.035	0.030	0.038	0.013	1.767
Al^{VI}	0.458	0.463	0.456	0.472	0.719
Ti	0.004	0.004	0.004	0.006	0.087
Cr	0.001	0.002	0.002	0.001	0.015
Fe^{3+}	0.010	0.000	0.041	0.000	0.448
Fe^{2+}	0.085	0.095	0.052	0.091	0.721
Mn	0.002	0.001	0.000	0.001	0.008
Mg	0.454	0.444	0.450	0.440	3.001
Ca	0.545	0.548	0.527	0.517	1.636
Na	0.441	0.443	0.467	0.472	1.132
K	0.000	0.000	0.000	0.000	0.007
Ca-Tsch	0.031	0.026	0.035	0.007	
Opx	0.014	0.009	0.005	0.011	
Jd	0.427	0.437	0.421	0.465	
Hd	0.081	0.092	0.051	0.087	
Di	0.431	0.429	0.441	0.423	
Rest	0.017	0.007	0.047	0.008	

Zone II (Fig. 3f) is characterized by the presence of the oriented SiO_2 precipitates and shows lower concentrations of Al in the tetrahedral sites of the clinopyroxene structure ($Al^{IV} = 0.03$ cat., see Table 2, analysis no. 22). The content of Al^{IV} in omphacite enriched with SiO_2 precipitates, calculated on the basis of the integral microprobe analysis (the electron beam of 30 μm in diameter), is even lower and corresponds to 0.01 Al per formula unit (Table 2, analysis no. 6 N). Zone III is slightly enriched in Ca (see Fig. 3d) and depleted in Na. Zones I, II and III correspond to the metamorphic Stages I, II and III, respectively, in which Stage II is subdivided into parts IIa and IIb based on calculations that do and do not include the SiO_2 precipitates in the pyroxene structure. In some cases, direct contact is observed between Zones I and III, suggesting that the process leading to irregularly shaped grains was a dissolution event occurring between Stages II and III.

We can imagine that Zone II once surrounded Zone I completely according to a regular growth zonation typical for many garnet in metamorphic rocks. If this would have been true, the different thickness of Zone II around I and especially the contact of Zone III with Zone I would mean that a considerable portion of Zone II (and probably some of Zone I) was removed before Zone III grew around the remaining omphacite.

Calculated concentration of tetrahedrally co-ordinated Al^{IV} and Fe^{3+} along a profile through the omphacite grain (Omphacite no. 2a) is shown on Fig. 4a,b. The profile (Fig. 4a) clearly demonstrates chemical zonation in the omphacite. For example, Al^{IV} content in the centre (Stage I) of the grain is 0.04 p.f.u. while in the intermediate zone (Stage II) Al^{IV} content is as low as 0.03 p.f.u. (Stage IIa and Stage IIb cannot be differentiated here). Below it is demonstrated that the amount of Al^{IV} is lower than 0.03 p.f.u when the SiO_2 rods were analysed together with the host omphacite by a broader beam (see analysis 6 N, Table 2). Close to the rim zone of the omphacite (Stage III) Al^{IV} content again approaches 0.04 p.f.u. Fe^{3+} scatters much more strongly than Al^{IV}.

Other minerals

Rutile is a minor but primary eclogitic mineral that appears as inclusions in the various garnet and omphacite zones. EDS spectra record only a Ti peak as well as a small oxygen peak. Occasionally, omphacite is partially replaced by fine-grained clinopyroxene–plagioclase symplectites and/or by relatively coarse-grained (up to 0.2 mm) greenish to brownish amphibole intergrown with plagioclase. Amphibole is also variable in composition, which can be recognized from variations in colour within single grains. A growth zonation of amphibole might be expected. Typical amphibole compositions correspond to pargasitic hornblende (see Table 2).

GEOTHERMOBAROMETRY

Methods

To decipher the *P–T* conditions of the four stages of metamorphism (I, IIa, IIb, and III) two geothermobarometric methods have been applied. For geothermometry, the classical Fe^{2+}–Mg exchange reaction for the garnet–omphacite pair was chosen, which has been studied extensively and which is based on the following underlying equilibrium of components of these two phases:

$$\text{almandine} + 3\ \text{diopside} = \text{pyrope} + 3\ \text{hedenbergite} \qquad (1)$$

For the calculations (Table 3), five of the several available formulations have been selected for this system, calibrated by Råheim & Green (1978), Ellis & Green (1979), Powell (1985), Krogh (1988) and Ai (1994).

For geobarometry, we considered the change of Al from tetrahedral sites to octahedral sites which is pressure dependent for many different mineral parageneses. For the pair garnet-omphacite, the following equilibrium can be formulated considering components of these phases:

$$2\ \text{grossular} + \text{pyrope} = 3\ \text{diopside} + 3\ CaAl_2SiO_6 \qquad (2)$$

The *P–T* location of this equilibrium for given garnet and omphacite compositions was thermodynamically calculated using the GeO-Calc computer program package of Brown *et al.*, (1988). The thermodynamic data for the participating components and the solid solution models for garnet and omphacite were reported by Massonne (1992, 1995) who previously considered the above equilibrium for the derivation of these thermodynamic data from experimental results. The GeO-Calc program also allows simultaneous calculation of equilibrium (1) (see Fig. 5), as well as the equilibrium:

$$2\ \text{grossular} + \text{almandine} = 3\ \text{hedenbergite} + 3\ CaAl_2SiO_6 \qquad (3)$$

However, the latter is not an independent constraint because of eq. (3) = eq. (1) − eq. (2).

Figure 5 shows that there is a significant temperature dependence of eq. (2); d*T*/d*P* *c.* 200 °C/GPa (in contrast, for eq. (1), d*T*/d*P* *c.* 40 °C/GPa). This fact, coupled with the low concentration of $CaAl_2SiO_6$ component in omphacite, makes pressure estimates sensitively dependent on the accuracy of determination of the $CaAl_2SiO_6$ component. Being aware of this problem, all possible efforts were made to analyse the omphacite compositions precisely, for instance by repeated checks of the microprobe standards during the analytical procedure. Despite this care, the barometry calculations based upon calcium–Tschermak's component are semiquantitative at best; the determinations here are estimated to have errors for the absolute pressure values probably in the range of ±0.5 GPa. However, this is the only geobarometer available for this system. It is worthy of note that Sabau (2000) applied the above barometer to eclogites of the Leaota Mountains, Southern Carpathians and obtained reasonable results.

In principle, temperatures also can be estimated from the Ti content of garnet using the preliminary calibration of Massonne & Brandelik (1998). This method is related to the equilibrium:

$$\text{pyrope} + 3\ \text{rutile} = Mg_3Al_2Ti_3O_{12} + 3\ SiO_2 \qquad (4)$$

However, because of the absence of coexisting quartz or coesite in association with rutile and garnet, only maximum temperatures can be calculated by this method.

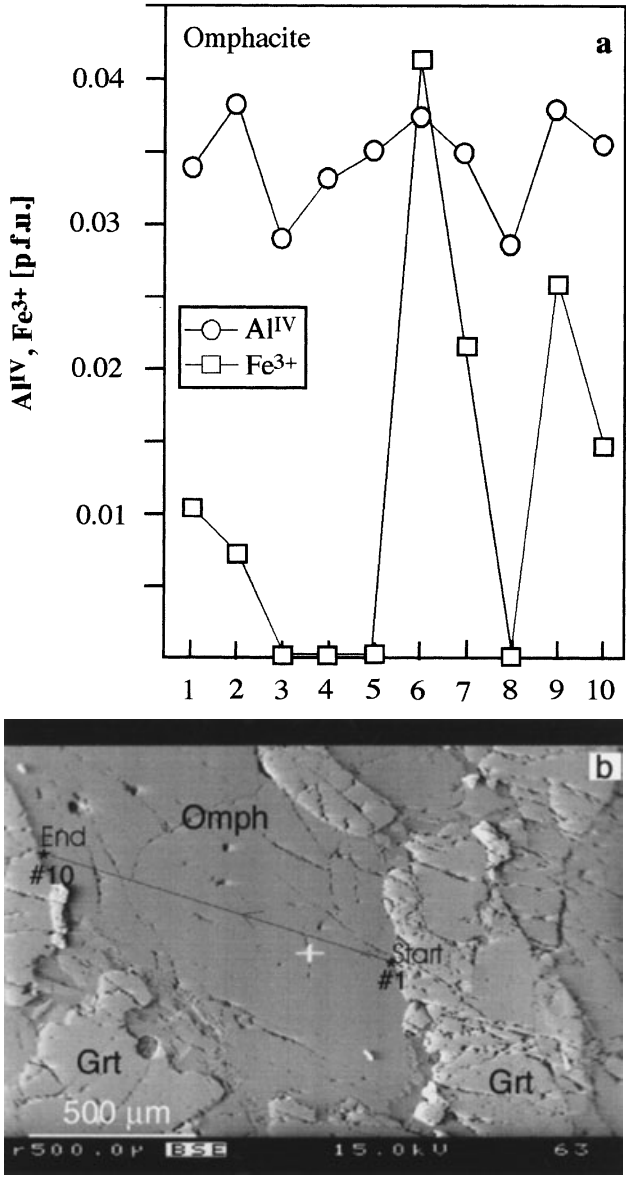

Fig. 4. Calculated concentrations of tetrahedrally co-ordinated $Al = Al^{IV}$ and Fe^{3+} (a) on the basis of 10 full analyses obtained with the electron microprobe along a profile through omphacite (b).

Result of calculations

Our analytical studies suggest that garnet-omphacite pairs chosen for *P–T* calculations were in equilibrium during at least three stages of metamorphism. In order to acquire as much insight as possible into Stage II, the *P–T* calculations were made for the omphacite composition directly measured with a normal microprobe beam, avoiding the quartz rods, and for the bulk pyroxene composition measured with a 30-μm diameter beam in order to integrate the quartz rods into the omphacite composition. The silica-rich composition obviously preceded the exsolution process, hence for consistency in a time sense, we have labelled the integrated composition 'Stage IIa' (a progressive stage) and the current pyroxene composition 'Stage IIb' (a retrogressive stage).

Metamorphic conditions were estimated in two ways: (i) temperatures were estimated from the various

Table 3. Temperature (°C) estimates using the $Fe^2 \pm Mg^{2+}$ exchange between garnet and clinopyroxene according to different works. The selection of analyses for coexisting garnet and omphacite is explained in the text.

	Pressure [GPa]	Ai (1994)	Ellis & Green (1979)	Krogh (1988)	Powell (1985)	Råheim & Green (1978)
Stage I (core analyses)						
omphacite analysis no. 25	2	584	691	653	671	615
garnet analysis no. 16	4	690	747	712	725	739
Stage II						
omphacite analysis no. 22	2	743	829	806	812	744
garnet analysis no. 9	4	864	887	868	867	880
Stage III (rim analyses)						
omphacite analysis no. 20	2	624	721	678	700	688
garnet analysis no. 19	4	736	775	735	752	816

calibrations of the Fe^{2+}–Mg exchange thermometer based upon assumed pressures of 2.0 and 4.0 GPa (Table 3); (ii) pressures and temperatures were estimated by combining the three mineral reactions given in Table 4 and shown on Fig. 5. In the former case, only the current composition of pyroxene and garnet as measured by EMP (Stages I, IIb, III) were considered, whereas in the latter case, we separately considered the present composition of omphacite for Stage IIb, and the broad-beam, integrated, composition for Stage IIa. These data taken together indicate a relatively low temperature of *c.* 700 °C at a pressure close to 2.4 GPa for Stage I, followed by a dramatic increase in both pressure and temperature. The minimum *P–T* fit for Stage II is provided by Stage IIb (*c.* 900 °C; 3.7 GPa), in which the SiO_2 exsolution from the omphacite is ignored. When the pyroxene composition is corrected for SiO_2 exsolution, however, the result (Stage IIa) is *c.* 1100 °C; 7 GPa. Although we cannot unambiguously distinguish whether the coexisting garnet composition was set before or after SiO_2 exsolution, the calculated pressure is quite insensitive to garnet composition; it is primarily driven by the reallocation of more Al to octahedral sites caused by the greater SiO_2 content of the pyroxene. The subsequent *P–T* evolution is characterized by a return to much lower pressures accompanied by a moderate temperature decrease (*c.* 750 °C; 2.1 GPa). The average temperature calculated from the various calibrations for the $Fe^2 \pm Mg$ exchange thermometer is about 70 °C lower at a given pressure than the ones thermodynamically calculated. As a consequence, if the latter thermometer is more accurate than the thermodynamical calculations, the metamorphic *P–T* path shown on Fig. 6 would be shifted to somewhat lower temperatures.

Although no free silica (other than the SiO_2 precipitates) was observed in the studied samples, the method of Massonne & Brandelik (1998) was applied and obtained temperatures similar to those given above.

The tiny oriented TiO_2 needles observed in garnet might be a product of exsolution following Stage IIa. If so, they would point to higher temperatures for Stage IIa. However, such TiO_2 needles are abundant in garnet from many low- to medium temperature eclogites and some previous workers have interpreted such inclusions as relics of a phase relatively rich in Ti that was more or less completely digested by Ti-poor garnet (e.g. Vogel, 1967). More data will be needed before this observation can be readdressed productively.

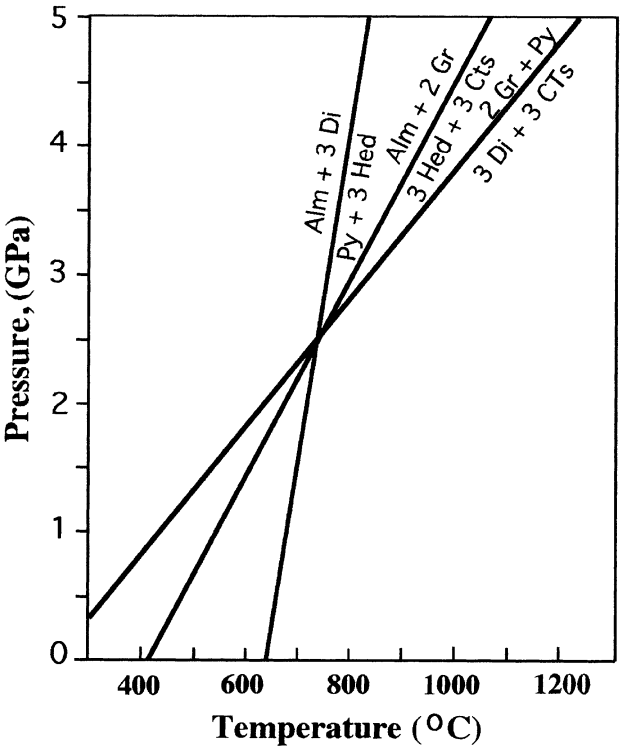

Fig. 5. Relative position of equilibrium curves calculated for geothermobarometry in a *P–T* diagram. Abbreviations: Alm = almandine, CTs = $CaAl_2SiO_6$, Di = diopside, Gr = grossular, Hed = hedenbergite, Py = pyrope. The example is related to the calculated *P–T* conditions (= intersection of the curves) of metamorphic Stage I.

DISCUSSION

Petrographic and compositional observations of the minerals of the AA eclogites suggest that the rocks were subjected to at least four stages of metamorphism. The earliest recorded equilibration, Stage I,

Table 4. *P–T* estimates for stages I to III by calculating the invariant point where the curves of the mineral equilibria: almandine (Alm) + 2 grossular = 3 hedenbergite + 3 $CaAlAlSiO_6$; 2 grossular (Grs) + pyrope = 3 diopside (Di) + 3 $CaAlAlSiO_6$; (CTs) almandine + 3 diopside = pyrope (Prp) + 3 hedenbergite (Hd) intersect (see Fig. 5). For the thermodynamic calculation the data of Massonne (1995) were used assuming that omphacite crystallized as C2/c modification. The analyses numbers for the garnet-omphacite pair selected are given in Table 3. For Stage IIb the 30 μm beam diameter analyses of omphacite enriched with SiO_2 precipitates was used instead of omphacite 22 (see Table 2 and 6 N – integral analysis).

	T (°C)	P (GPa)
Stage I	727	2.36
Stage IIa	1118	7.04
Stage IIb	950	3.7
Stage III	760	2.12

is calculated to be at 700 °C; 2.4 GPa. The peak of metamorphism recorded in the rocks corresponds to Stage IIa, *c.* 1100 °C; 7 GPa, followed by profound decompression to *c.* 900 °C; 3.7 GPa (Stage IIb). The latter estimate is in good agreement with calculations of Ernst (1977) for samples collected from the same eclogite body ($T = 900$ °C at $P = 4$ GPa). This is an excellent correspondence because previous workers were unaware of the former presence of silica-rich omphacite in these rocks. Stage III equilibration occurred at retrograde conditions close to those of Stage 1 ($T = 750$ °C, $P = 2.1$ GPa).

Given that the conditions calculated from thermobarometry are much more sensitive to changes in pyroxene chemistry than to changes in garnet chemistry, Stage IIa can be viewed as an approximate measure of the highest recorded stage of metamorphism whereas Stage IIb is a re-equilibration during exhumation, after exsolution of the SiO_2 rods. Although AA eclogite and AA garnet peridotite clearly have a tectonic contact, at least in part (emphasized by the presence locally of late blastomylonites between them; Möckel, 1969), Fig. 6 shows that there is a marked similarity in the trajectory of their *P–T* paths during exhumation from approximately 200 km. Our exhumation curve for AA eclogite is in good agreement with the equilibration points calculated for the peridotite by Ernst (1977) and by Medaris & Carswell (1990), but at pressures >4 GPa (120 km), the eclogite curve is cooler than that suggested for the AA peridotite by Brenker & Brey (1997), and much cooler than that suggested by Paquin & Altherr (2001a). The combined peridotite and eclogite exhumation curves are also compatible with the deeper constraints presented by Dobrzhinetskaya *et al.* (1996, 2000a), Bozhilov *et al.* (1999), and Green *et al.* (2000).

Our results are also consistent with the data of Nimis & Trommsdorff (2001a), but not their arguments. These authors concluded that the relatively low pressure and temperature equilibration point that they calculated (3.2 ± 0.3 GPa; 844 ± 33 °C) is the absolute maximum set of conditions experienced by the AA peridotite. Our eclogite Stage IIb, which is clearly retrograde after Stage IIa, yields *P–T* conditions nominally somewhat higher than those of Nimis & Trommsdorff (2001a), but within reasonable error bounds are indistinguishable from their calculations. Indeed, correction by Nimis & Trommsdorff (2001a p. 111) of Brenker & Brey's pyroxene compositions for the pigeonite lamellae reported by Bozhilov *et al.* (1999) led them to *P–T* conditions virtually identical to those we determined for Stage IIb. Our results on AA eclogite and the numerous thermobarometric and microstructural results indicating higher pressures for the AA peridotite suggest that Nimis & Trommsdorff (2001a) have probably well-measured the prominent late Alpine overprint that is clearly present in these rocks, and that others have sampled various parts of an older, higher-pressure, history.

The other recent paper focused on the *P–T* history of these rocks, that of Paquin & Altherr (2001a), investigated in detail the major and minor element geochemistry of several samples of AA peridotite and concluded that garnet had been thoroughly recrystallized at *c.* 6 GPa, 1200 °C, after which they proposed it experienced an isothermal (superadiabatic!) decompression of more than 4 GPa followed by an isobaric cooling. There are many fundamental discrepancies between the results of Nimis & Trommsdorff (2001a) and Paquin & Altherr (2001a). Many of those discrepancies are addressed in their recent discussion and reply (Nimis & Trommsdorff, 2001b; Paquin & Altherr, 2001b) and need not be discussed further here.

Our calculation of 7 GPa for AA eclogite has a significant error associated with it ($\pm$ at least 0.5 GPa), hence the maximum pressure evidence in the eclogite could be consistent with the pressure estimate of Paquin & Altherr (2001a) for the peridotite. Indeed, at a pressure of 7 GPa, a small majoritic component would be expected in the associated garnet, which is not observed, hence we view 7 GPa as an upper limit for Stage IIa. However, the temperatures derived from the thermobarometric analysis could not possibly be consistent with a decompression history at the high temperatures proposed by Paquin & Altherr (2001a). As a consequence, either the AA peridotite and eclogite were commingled in the Alpine subduction zone only at relatively low pressures, or one of these two exhumation histories must be in error.

Setting aside this discrepancy, we find that all other previous results on the exhumation history of the AA eclogite and AA peridotite are consistent from depths of at least 120 km (4 GPa). Integrating the new results presented here with our previously published observations suggesting exhumation of the AA peridotite from significantly greater depths, we propose two possible scenarios: (i) if the high-temperature equilibration at 5–6 GPa calculated by Brenker & Brey (1997) and by Paquin & Altherr (2001a) is correct, it would appear

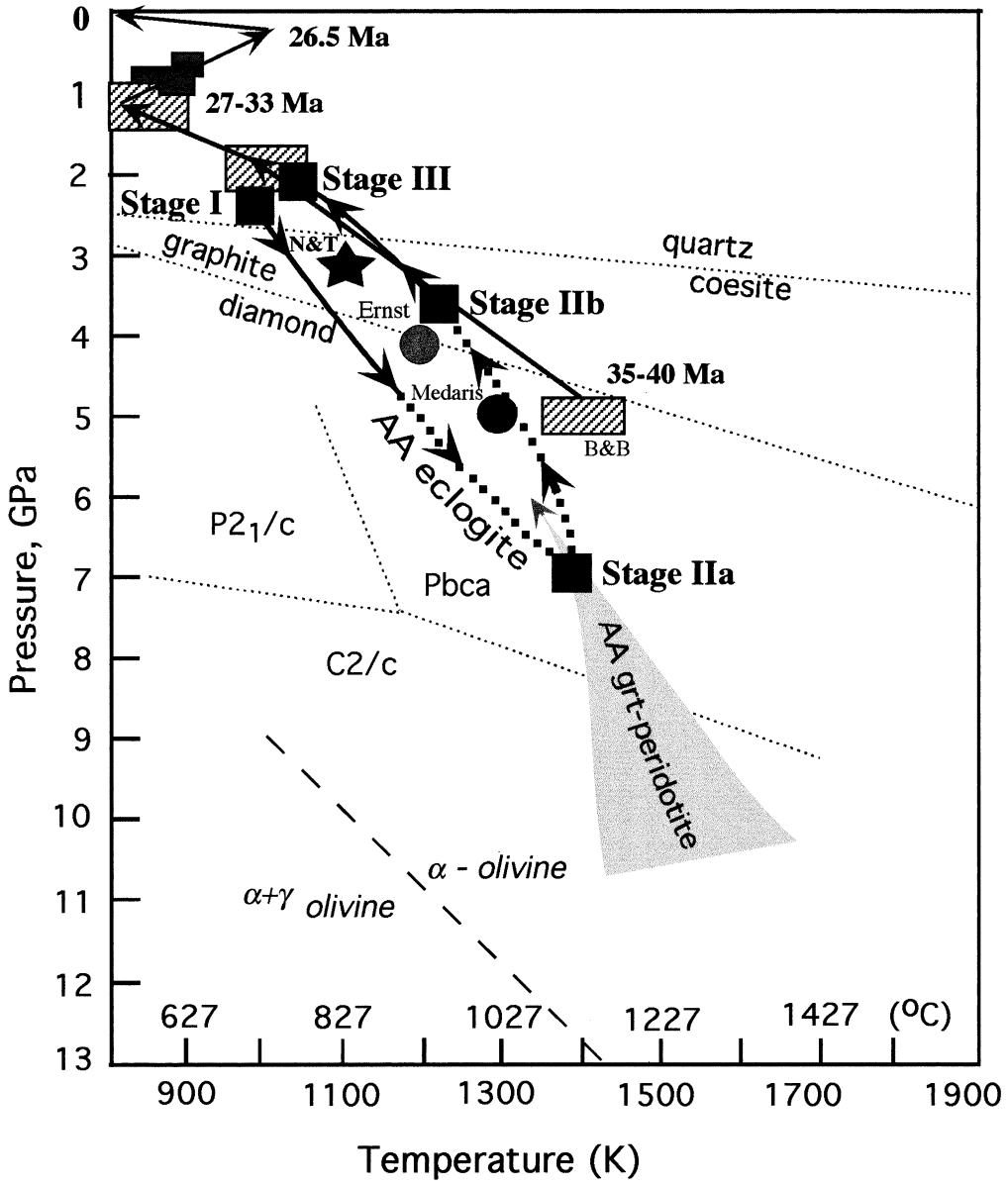

Fig. 6. *P–T* diagram showing constraints on the exhumation path of the Alpe Arami eclogite and garnet peridotite. Filled squares correspond to *P–T* conditions of eclogite containing omphacite with SiO_2 precipitates determined by this research as Stages I, IIa, IIb and III. Black solid and dashed lines with solid arrowheads show a possible *P–T* path of the eclogite. Grey and black solid circles present maximum metamorphic conditions determined for garnet peridotite and eclogite by Ernst (1977, 1978, 1981), and by Medaris & Carswell (1990) for garnet peridotite, respectively, using thermobarometry. Rectangular hatched (B & B) and smaller grey boxes connected by grey solid arrows are from Brenker & Brey (1997). Grey segment is a field which contains the possible exhumation path for garnet peridotite according to Dobrzhinetskaya *et al.* (1996, 2000) and Bozhilov *et al.* (1999). Solid star (N & T) – maximum *P–T* conditions determined by Nimis & Trommsdorff (2001a) for garnet peridotite. Olivine phase equilibria from Akaogi *et al.* (1989). The $(Mg_{0.9},Fe_{0.1})SiO_3$ phase diagram is from Woodland & Angel (1997).

that the AA eclogite was probably subducted to depths of at least 180 km in the Alpine subduction zone and was brought into contact with the AA peridotite during exhumation at a depth of 150 km or less; (ii) if the high temperature results cannot be substantiated by subsequent work, the entire body of data remain consistent with a single exhumation event from depths perhaps greater than 300 km. It would appear, however, that many aspects of the histories of these fascinating and complicated bodies remain to be elucidated, including the depth at which they came into juxtaposition.

The critically important new information provided to the Alpe Arami 'problem' by the results presented here is that a prograde stage of metamorphism is recorded in the eclogites, that a subsequent rapid subduction to great depth and return is indicated by preservation of the clearly discernible zonation patterns of the minerals, including exsolution of SiO_2 from omphacite, and that at depths greater than *c.* 120 km, the history of the eclogites may have been different from that of the peridotite.

ACKNOWLEDGEMENTS

We thank K. Bozhilov for helpful discussions. A field trip to the Alps for L.D. to collect eclogite samples was partly supported by NSF grant EAR96-283432. L.D. also thanks Stuttgart University for financial support for travel during her visit in 2000. We express

our appreciation to G. Ernst (Stanford University, USA) and E. Eide (Norwegian Geological Survey) for thoughtful and detailed reviews.

REFERENCES

Ai, Y., 1994. A revision of the garnet-clinopyroxene Fe^{2+}–Mg exchange geothermometer. *Contributions to Mineralogy and Petrology*, **115,** 467–473.

Akaogi, M., Ito, E. & Navrotsky, A., 1989. Olivine modified spinel-spinel transition in the system Mg_2SiO_4–Fe_2SiO_4: calorimetric measurements, thermochemical calculation, and geophysical application. *Journal of Geophysical Research*, **94,** 15671–15685.

Angel, R. J., Gasparik, T., Ross, N. L., Finger, L. W., Prewitt, C. T. & Hazen, R. M., 1988. A silica-rich pyroxene phase with six-coordinated silicon. *Nature*, **335,** 156–158.

Arlt, Th, Kunz, M., Stolz, J., Armbruster, Th & Angel, R. J., 2000. P-T-X data on P21/c-clinopyroxenes and their displacive phase transitions. *Contributions to Mineralogy and Petrology*, **138,** 35–45.

Bakun-Chubarow, N., 1992. Quartz pseudomorphs after coesite and quartz exsolutions in eclogitic omphacites of the Zlote Mountains in the Sudetes (SW Poland). *Archiwum Miner*, **48,** 3–25.

Bernhardt, H. J., Massonne, H.-J., Reinecke, T., Reinhardt, J. & Willner, A. P., 1995. Digital element distribution maps, an aid for petrological investigations. *European Journal of Mineralogy*, **7,** 28–30.

Bozhilov, K., Green, H. W. & Dobrzhinetskaya, L. F., 1999. Clinoenstatite in Alpe Arami peridotite: additional evidence of very high pressure. *Science*, **284,** 128–132.

Brenker, F. E. & Brey, G. P., 1997. Reconstruction of the exhumation path of the Alpe Arami garnet-peridotite body from depths exceeding 160 km. *Journal of Metamorphic Geology*, **15,** 581–592.

Brown, T. H., Berman, R. G. & Perkins, E. H., 1988. Geo-Calc: Software package for calculation and display of pressure-temperature-composition phase diagrams using an IBM or compatible Personal Computer. *Computers in Geosciences*, **14,** 279–289.

Buiskool Toxopeus, J. M. A., 1977. Fabric development of olivine in a peridotite mylonite. *Tectonophysics*, **39,** 55–71.

Dobrzhinetskaya, L., Bozhilov, K. N. & Green, H. W. I. I., 2000a. The solubility of TiO_2 in olivine: implications for the antle wedge environment. *Chemical Geology*, **163,** 325–338.

Dobrzhinetskaya, L. F. & Green, H. W., Massonne, H.-J. & Schweinehage, R., 2000b. Silica precipitates in omphacite from eclogite at Alpe Arami, Switzerland: an evidence of deep subduction. *Eos, Transaction, AGU Fall Meeting, (Abstract)*, **81,** F1261.

Dobrzhinetskaya, L. F., Eide, E., Korneliussen, A., Larsen, R., Millege, J., Posukhova, T. V., Smith, D. S., Sturt, B. A., Taylor, W. R. & Trönnes, R. G., 1995. Diamond in metamorphic rocks of the Western Gneiss Region in Norway. *Geology*, **23,** 597–600.

Dobrzhinetskaya, L. F., Green, H. W. I. I. & Wang, S., 1996. Alpe Arami: a peridotite massif from depths of more than 300 kilometers. *Science*, **271,** 1841–1845.

Ellis, D. J. & Green, D. H., 1979. An experimental study of the effect of Ca upon garnet-clinopyroxene Fe-Mg exchange equilibria. *Contributions to Mineralogy and Petrology*, **71,** 13–22.

Ernst, W. G., 1977. Mineralogic study of eclogitic rocks from Alpe Arami, Lepontine Alps, Southern Switzerland. *Journal of Petrology*, **18,** 371–398.

Ernst, W. G., 1978. Petrochemical study of lherzolitic rocks from Western Alps. *Journal of Petrology*, **19,** 341–392.

Ernst, W. G., 1981. Petrogenesis of eclogites and peridotites from the Western and Ligurian Alps. *American Mineralogist*, **66,** 443–472.

Evans, B. W. & Trommsdorff, V., 1975. Gradation between eclogite and metarodingite, Ticino, Switzerland. *Geological Society of America (Abstracts with Programs)*, **7,** 1069–1070.

Gayk, T., Kleinschrodt, R., Langosch, A. & Seidel, E., 1995. Quartz exsolution in clinopyroxene of high-pressure granulite from the Münchberg massif. *European Journal of Mineralogy*, **7,** 1217–1220.

Green, H. W., Dobrzhinetskaya, L. F. & Bozhilov, K. N., 2000. Mineralogical and experimental evidence for very deep exhumation from subduction zones. *Journal of Geodynamics*, **30,** 61–76.

Grubenmann, U., 1908. Der Granatolivinfels des Gordunotales und seine Begleitgesteine. *Vierteljahresschrift Naturforshung Gesellschaft, Zürich*, **53,** 129–156.

Katayama, I., Parkinson, C. D., Okamoto, K., Nakajima, Y. & Maruyama, S., 2000. Supersilic clinopyroxene and silica exolutions in UHPM eclogite and pelitic gneiss from the Kokchetav massif, Kazakhstan. *American Mineralogist*, **85,** 1368–1374.

Krogh, E. J., 1988. The garnet-clinopyroxene Fe-Mg geothermometer – a reinterpretation of existing experimental data. *Contributions to Mineralogy and Petrology*, **99,** 44–48.

Mao, H. K., 1971. The system jadeite ($NaAlSi_2O_6$) – anorthite ($CaAl_2Si_2O_8$) at high pressures. *Carnegie Institute Year Book*, **69,** 163–168.

Massonne, H.-J., 1992. Thermochemical determination of water activities relevant to eclogitic rocks. In: *Water–Rock Interaction WRI×7. Proceedings of the 7th International Symposium* (eds Kharaka, Y. K. & Maest, A.), pp. 1523–1526. A. A. Balkema, Rotterdam.

Massonne, H.-J., 1995. Experimental and petrogenetic study of UHPM. In: *Ultrahigh Pressure Metamorphism* (eds Coleman, R. G. & Wang, X.), pp. 33–95. Cambridge University Press, Cambridge.

Massonne, H.-J., 1999. A new occurrence of microdiamonds in quartzofeldspathic rocks of the Saxonian Erzgebirge, Germany, and their metamorphic evolution. In: *Proceedings of the VIIth International Kimberlitic Conference* (eds Gurney, J. J., Gurney, J. L., Pascoe, M. D. & Richardson, S. H.), pp. 533–539. Red Roof Desing cc, Cape Town.

Massonne, H.-J. & Brandelik, A., 1998. Ti in Al-garnet – a newly calibrated geothermobarometer for high-pressure and ultra-high-pressure metamorphic rocks. *Eos, Transaction, AGU Fall Meeting, (Abstract)*, **79,** F972.

Medaris, L. G. & Carswell, D. A., 1990. The petrogenesis of Mg-Cr garnet peridotites in European metamorphic belts. In: *Eclogite Facies Rocks* (ed. Carswell, D. A.), pp. 260–290. Blackie, London.

Möckel, J. R., 1969. Structural petrology of the garnet peridotite of Alpe Arami (Ticino, Switzerland). *Leidse Geologische Mededelingen*, **42,** 61–130.

Nimis, P. & Trommsdorff, V., 2001a. Revised thermobarometry of Alpe Arami and other garnet peridotites from the central Alps. *Journal of Petrology*, **42,** 103–115.

Nimis, P. & Trommsdorff, V., 2001b. Comment on 'New Constraints on the *P–T* evolution of the Alpe Arami garnet peridoite body (Central Alps, Switzerland)' by Paquin & Altherr (2001). *Journal of Petrology*, **42,** 1773–1779.

O'Hara, M. J. & Mercy, E. L. P., 1963. Petrology and petrogenesis of some garnetiferous peridotites. *Transactions of the Royal Society of Edinburgh*, **65,** 251–314.

Paquin, J. & Altherr, R. 2001a. New constraints on the P–T evolution of the Alpe Arami garnet peridoite body (Central Alps, Switzerland). *Journal of Petrology*, **42,** 1119–1140.

Paquin, J. & Altherr, R. 2001b. New constraints on the P–T evolution of the Alpe Arami garnet peridoite body (Central Alps, Switzerland)': Reply to Comment by Nimis & Trommsdorff (2001). *Journal of Petrology*, **42,** 1781–1787.

Powell, R., 1985. Regression diagnostics and robust regression in geothermometer/geobarometer calibration: the garnet-clinopyroxene geothermometer revisited. *Journal of Metamorphic Geology*, **3,** 231–243.

Råheim, A. & Green, D. H., 1978. Experimental determination of the temperature and pressure dependence of the Fe-Mg partition coefficient for coexisting garnet and clinopyroxene. *Contribution to Mineralogy and Petrology*, **48,** 179–203.

Risold, A.-C., Trommsdorff, V. & Grobéty, B., 2001. Genesis of ilmenite rods and palisades along humite-type defects in olivine from Alpe Arami. *Contribution to Mineralogy and Petrology*, **140,** 619–628.

Sabau, G., 2000. A possible UHP-eclogite in the Leaota Mts. (South Carpathians) and its history from high pressure melting to retrograde inclusion in a subduction melange. *Lithos*, **52,** 235–276.

Smith, D. S., 1988. A review of the peculiar mineralogy of the Norwegian coesite-eclogite province, with crystal-chemical. Petrological, geochemical and geodynamical notes and an extensive bibliography. In: *Eclogite and Eclogite-Facies Rocks* (ed. Smith, D. C.), pp. 1–206. Elsevier, Amsterdam.

Smith, D. S. & Cheeney, R. F., 1980. Oriented needles of quartz in clinopyroxene: evidence for exolution of SiO_2 from a non-stoichiometric supersilicic 'clinopyroxene'. *26th International Geol Congress (Abstract Volume)*, p. 145. Elsevier, Amsterdam.

Smyth, J. R., 1980. Cation vacancies and the crystal chemistry of breakdown reactions in kimberlitic omphacites. *American Mineralogist*, **65,** 1185–1191.

Sobolev, N. V. & Shatsky, V., 1990. Diamond inclusions in garnets from metamorphic rocks: a new environment of diamond formation. *Nature*, **343,** 742–746.

Trommsdorff, V., Evans, B. W. & Richter, W., 1975. Eklogit-Rodingit Übergänge in Ultramafititen der Cima Lunga Serie. *Schweizerische Mineralogische und Petrographische Mitteilungen*, **55,** 572–575.

Tsai, C. H., 1998. Petrology and geochemistry of mafic-ultramafic rocks in the north of the Dabie complex, central-eastern China. *PhD Thesis*, *Stanford University, Stanford.*

Van Roermund, H. L. M. & Drury, M. R., 1999. Ultra-high pressure ($P > 6$ GPa) garnet peridotites in Western Norway: exhumation of mantle rocks from >185 km depth. *Terra Nova*, **10,** 295–301.

Vogel, D. E., 1967. Petrology of an eclogite- and pyrigarnite-bearing polymetamorphic rock complex at Cabo Ortegal, NW Spain. *Leidse Geologische Mededelingen*, **40,** 121–213.

Wood, B. J. & Henderson, C. M. B., 1978. Compositions and unit-cell parameters of synthetic non-stoichiometric tschermakitic clinopyroxene. *American Mineralogist*, **63,** 66–72.

Woodland, A. B. & Angel, R. L., 1997. Reversal of the orthoferrosilite-high-pressure clinoferrosilite transition, a phase diagram for $FeSiO_3$ and implications for the mineralogy of the Earth's upper mantle. *European Journal of Mineralogy*, **9,** 245.

Xu, S., Okay, A. I., Sengor, A., Su, W., Liu, Y. & Jiang, L., 1992. Diamond from the Dabie Shan metamorphic rocks and its implication for tectonic setting. *Science*, **256,** 80–82.

Yang, J., Godard, G., Kienast, J.-R., Lu, Y. & Sun, J., 1993. Ultrahigh-pressure (60 Kbar) magnesite-bearing garnet peridotites from northeastern Jiangsu, China. *Journal of Geology*, **101,** 541–554.

Ye, K., Cong, B. & Ye, D., 2000. The possible subduction of continental material to depths greater than 200 km. *Nature*, **407,** 734–736.

Zhang, R. Y., Hirajima, T., Banno, S., Cong, B. & Liou, J. G., 1995. Petrology of ultra-high pressure rocks from the southern Sulu region, eastern China. *Journal of Metamorphic Geology*, **13,** 659–675.

Zharikov, V. A., Ishbulatov, R. A. & Chudinovskikh, L. T., 1984. High-pressure clinopyroxene and the eclogite barier. *Geology and Geophysics*, **24,** 53–61.

Received 25 May 2001; revision accepted 8 January 2002.